Eighth International Conference on
ADVANCES IN STEEL STRUCTURES
Lisbon, Portugal, July 22-24, 2015

ESTIMATION OF ECONOMIC LOSSES IN SEISMIC-RESISTANT POST-TENSIONED STEEL FRAMES WITH VISCOUS DAMPERS

Theodore L. Karavasilis*, Athanasios I. Dimopoulos*, Angelos S. Tzimas*, George S. Kamaris* and Dimitrios Vamvatsikos**

* School of Engineering, University of Warwick, United Kingdom
e-mails: T.Karavasilis@warwick.ac.uk, A.Dimopoulos@warwick.ac.uk, A.Tzimas@warwick.ac.uk, G.Kamaris@warwick.ac.uk

** National Technical University of Athens, 15780 Athens, Greece
e-mail: Divamva@mail.ntua.gr

Keywords: Self-centering; dampers; steel frames; loss estimation; vulnerability functions; Eurocode 8; ATC-58; Collapse.

Abstract. *This paper evaluates the potential of self-centering moment-resisting frames (SC-MRFs) with viscous dampers to reduce the economic losses in steel buildings due to strong earthquakes. The evaluation is based on the comparison of different designs of a prototype steel building using as lateral-load resisting system: 1) conventional steel moment resisting frames (MRFs); 2) MRFs with viscous dampers; 3) SC-MRFs; and 4) SC-MRFs with viscous dampers. The economic losses of these four design cases are estimated by developing vulnerability functions according to the ATC-58 methodology. The influence of residual storey drifts on economic losses is examined, by accounting for the possibility of having to demolish a building as a result of excessive residual storey drifts. Results highlight the importance of considering residual story drifts as a demand parameter to economic loss estimation; and show that the use of viscous dampers significantly improves the building's performance for both SC-MRF and MRF, resulting in lower repair cost.*

1 INTRODUCTION

The February 2011 Christchurch earthquake confirmed that conventional seismic-resistant structures, such as steel moment-resisting frames (MRFs), experience difficult-to-repair damage due to inelastic deformations in main structural members, residual story drifts, and appreciable peak story drifts. After that earthquake, a significant percentage of the buildings in the central business area were declared unusable [1] with the reconstruction cost to be estimated approximately equal to 40 billion New Zealand dollars without considering the economic losses due to disruption of building use or occupation [2]. These loses highlight the need to use in practice more resilient structures that are less vulnerable and easier to repair after strong earthquakes with the goal of reducing, if not avoiding, economic seismic losses.

Steel self-centering moment-resisting frames (SC-MRFs) with post-tensioned (PT) beam-column connections are a class of resilient seismic-resistant structures that eliminate beam inelastic deformations and residual drifts. PT connections use yielding-based [3-9] or friction-based [10-13] energy dissipation devices, which are activated when gaps open and can be easily replaced if damaged. However, existing design procedures [14, 15] aim to achieve peak drifts similar to those of conventional steel MRFs, and so, accept appreciable damage in drift-sensitive non-structural elements.

Steel MRFs with passive dampers is another class of resilient structures that can reduce peak storey drifts, and indirectly, inelastic deformations in structural members. Previous

analytical and experimental research showed that it is generally not feasible to design steel MRFs with elastomeric dampers at a practical size to eliminate inelastic deformations in main structural members under the design basis earthquake (DBE) [16, 17]. To address this issue, a design strategy for steel MRFs, which isolates damage in removable steel energy dissipation devices and uses in parallel viscous dampers to reduce peak storey drifts, has been proposed in [18]. A study shows that supplemental viscous damping does not always ensure adequate reduction of residual drifts of yielding structures [19]. A recent work evaluates the seismic collapse resistance of steel MRFs with viscous dampers and shows that supplemental viscous damping does not always guarantee a better seismic collapse resistance when the strength of the steel MRF with dampers is equal or lower than 75% the strength of a conventional steel MRF [20].

The use of viscous dampers in parallel to self-centering precast concrete base rocking walls has been proposed as an effective way to control peak storey drifts and residual drifts [21]. The parallel combination of hysteretic and viscous energy dissipation along with a friction slip mechanism in series connected to the viscous energy dissipation mechanism was found to achieve high levels of seismic performance for self-centering systems [22]. A recent study [23] on seismic design and assessment of steel SC-MRFs with viscous dampers within the framework of Eurocode 8 (EC8) [24], shows that providing supplemental viscous damping to steel SC-MRFs is a very effective way to reduce structural and non-structural damage by simultaneously controlling beam plastic deformations, peak storey drifts, and residual story drifts.

Economic seismic loss can be rigorously estimated using procedures that quantify and propagate uncertainties such as the early one developed by Porter *et al.* [25] that uses nonlinear dynamic analyses at different seismic intensities, predicts damage at the component level using fragility functions, and finally estimates the building repair cost. This method was further developed to become the PEER (Pacific Earthquake Engineering Research) methodology [26] that is now known as the 2nd generation performance based earthquake engineering (PBEE-2). Early studies on PBEE-2 showed that component damageability and ground motion time histories have strong influence on loss uncertainty, while material properties and other uncertainties in the structural model may have relatively little influence [27, 28]. A critical review of PBEE-2 and examination of its limitations has been conducted by Gunay and Mosalam [29]. At present, the state-of-art in economic seismic loss estimation is described by the ATC-58 methodology [30] that adopts PBEE-2 along with a database of structural and non-structural component fragility functions and repair cost estimates. The aforementioned loss estimation methodologies estimate economic losses based on peak response quantities such as peak storey drift or peak floor accelerations (PFA), without consider the influence of residual storey drifts on economic losses.

Ramirez and Miranda [31] showed how the probability of having to demolish a building as the result of excessive residual storey drifts influences seismic loss estimation. They assumed a lognormal distribution for the probability of demolition conditioned on the residual storey drift, with a median of 0.015 and a logarithmic standard deviation of 0.3. Because there is limited data to accurately determine the parameters of this distribution, sensitivity analysis was conducted and showed that loss estimation is more sensitive to the median than the dispersion of the probability of demolition. Jayaram *et al.* [32] also considered the probability of having to demolish a building as the result of excessive residual storey drifts, to develop vulnerability functions for six tall buildings.

To the authors knowledge the potential of SC-MRFs and SC-MRFs with viscous dampers to reduce economic seismic losses by simultaneously controlling structural and non-structural damage has not been quantified yet. Such quantification is of particular interest to justify the increased cost and design complexity associated with combining and applying in practice the

post-tensioning and passive energy dissipation technologies. Moreover, the effect of the assumed residual storey drift limit value beyond which it is generally less expensive to rebuild a structure than to repair it, should be quantitatively evaluated. For instance, McMormck *et al.* [33] after extensive review of previous research in Japan concluded that 0.005 rad is an important engineering index in terms of permissible residual storey drift levels, based on functionality, construction tolerances, and safety. Nevertheless, the selection of permissible residual storey drift level depends on engineering judgement. The probability of collapse in the total economic loss should also be quantified, in comparison to conventional MRFs and MRFs with viscous dampers.

This paper evaluates the potential of SC-MRFs with viscous dampers to reduce the economic losses in steel buildings due to strong earthquakes. SC-MRFs are using the recently developed PT connection with web hourglass shape pins (WHPs) [7, 8]. The evaluation is based on the comparison of different designs of a prototype steel building using as lateral-load resisting system: 1) conventional steel moment resisting frames (MRFs); 2) MRFs with viscous dampers; 3) SC-MRFs; and 4) SC-MRFs with viscous dampers. The economic losses of these four design cases are estimated by developing vulnerability functions according to the ATC-58 methodology [30], which considers all repair costs associated with restoring the building to its original condition. The probability of demolition is also conditioned, by assuming different permissible residual storey drift levels. The results show the superior minimal damage performance of SC-MRFs with and without dampers compared to the corresponding conventional MRFs, resulting in lower repair cost; their superior collapse resistance; and the influence of permissible residual storey drifts on the economic losses of the current design cases.

2 SC-MRFs USING PT CONNECTIONS WITH WHPs

Figure 1(a) shows a SC-MRF using PT connections with WHPs and figure 1(b) show an exterior PT connection with WHPs. The PT connection with WHPs has been experimentally and numerically evaluated by Vasdravellis et al. [7, 8]. Two high strength steel bars located at the mid depth of the beam, one at each side of the beam web, pass through holes drilled on the column flanges. The bars are post-tensioned and anchored to the exterior columns. WHPs are inserted in aligned holes on the beam web and on supporting plates welded to the column flanges. Energy is dissipated through inelastic bending of the WHPs that have an optimized hourglass shape (figure 1(c)) with enhanced fracture capacity [34]. The beam web and flanges are reinforced with steel plates. The panel zone is strengthened with doubler and continuity plates. A fin plate welded on the column flange and bolted on the beam web is used for easy erection and resistance against gravity loads before post-tensioning. Slotted holes on the beam web ensure negligible influence of the fin plate on the PT connection hysteretic behaviour.

A discontinuous steel-concrete composite slab (details shown in figure 2) is used to avoid damage in the slab as the gaps in the PT connections open and close (see figure 3(b)), i.e. similar to the solutions proposed in [6, 15, 23]. Shear studs for composite action are welded only on the secondary beams. The slab discontinuity is achieved by using two angle sections sliding on the beam framing perpendicularly to the SC-MRF columns. The secondary beams and the slab are placed after post-tensioning. The slab diaphragm eliminates beam shortening, and so, the internal axial forces in the beams remain constant and equal to those due to initial post-tensioning of the PT bars. Any further increase in the PT bars forces due to elongation under gap opening is transferred to the beam-column interfaces by the slab diaphragm.

The connection behaviour is characterized by gap opening and closing in the beam-column interface as a result of the re-centering force in the PT bars. Figure 3(a) shows the free body diagram of an external PT connection where d_{1u} and d_{1l} are the distances of the upper and

lower WHPs from the center of rotation that is assumed to be at the inner edge of the beam flange reinforcing plates; d_2 is the distance of the PT bars from the center of rotation; T is the total force in both PT bars; $F_{WHP,u}$ and $F_{WHP,l}$ are the forces in the upper and lower WHPs; C_F is the compressive force in the beam-column interface; V_{C1u} and V_{C1l} are the shear forces in the upper and lower column, M is the PT connection moment, V is the beam shear force; and N is the horizontal clamping force that is transferred to the beam-column interface through the slab diaphragm and the beam. Figure 3(b) shows the SC-MRF expansion due to rotations θ in the PT connections.

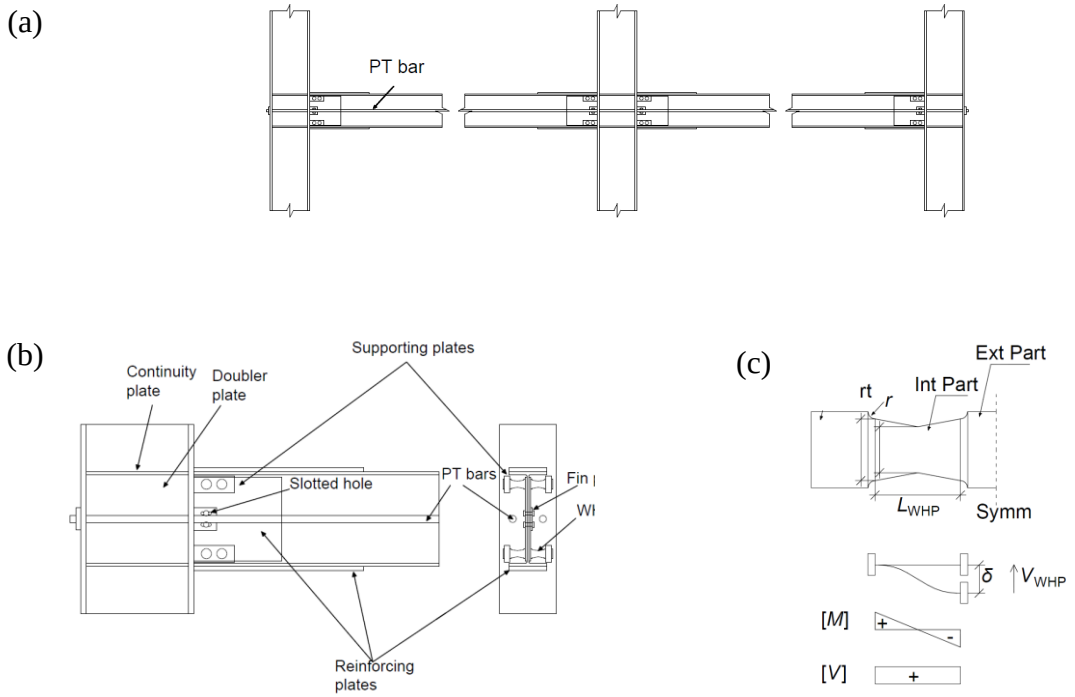

Figure 1: (a) SC-MRF; (b) exterior PT connection with WHPs; and (c) WHP geometry and assumed static system.

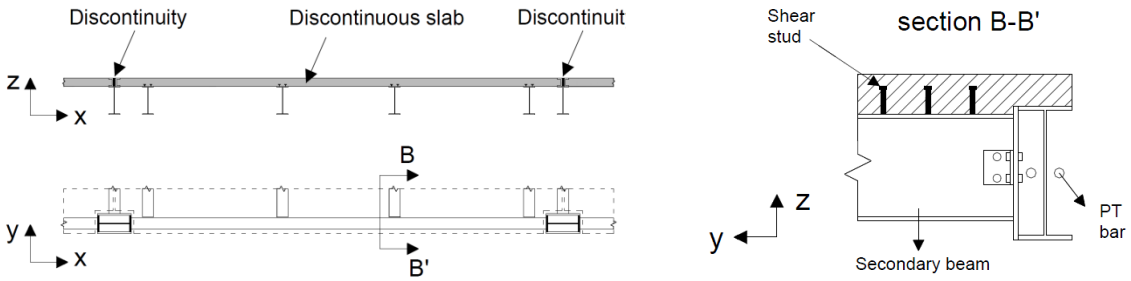

Figure 2: Discontinuous steel-concrete composite slab details.

Figure 3(c) shows the theoretical cyclic moment-rotation (M-θ) behaviour of the PT connection with WHPs, which has been verified by the large-scale experiments conducted by Vasdravellis et al. [7]. After decompression of the PT connection (Point 1 in Figure 3(c)), gap opens and the behaviour becomes nonlinear elastic with rotational stiffness S_1. At point 2, the upper WHPs yield and M continues to increase with slope S_2. At point 3, the lower WHPs yield and M continues to increase with slope S_3. When loading is reversed, the connection begins to unload until the gap closes. Equations to calculate S_1 to S_3 and θ_1 to θ_3 are provided in [23].

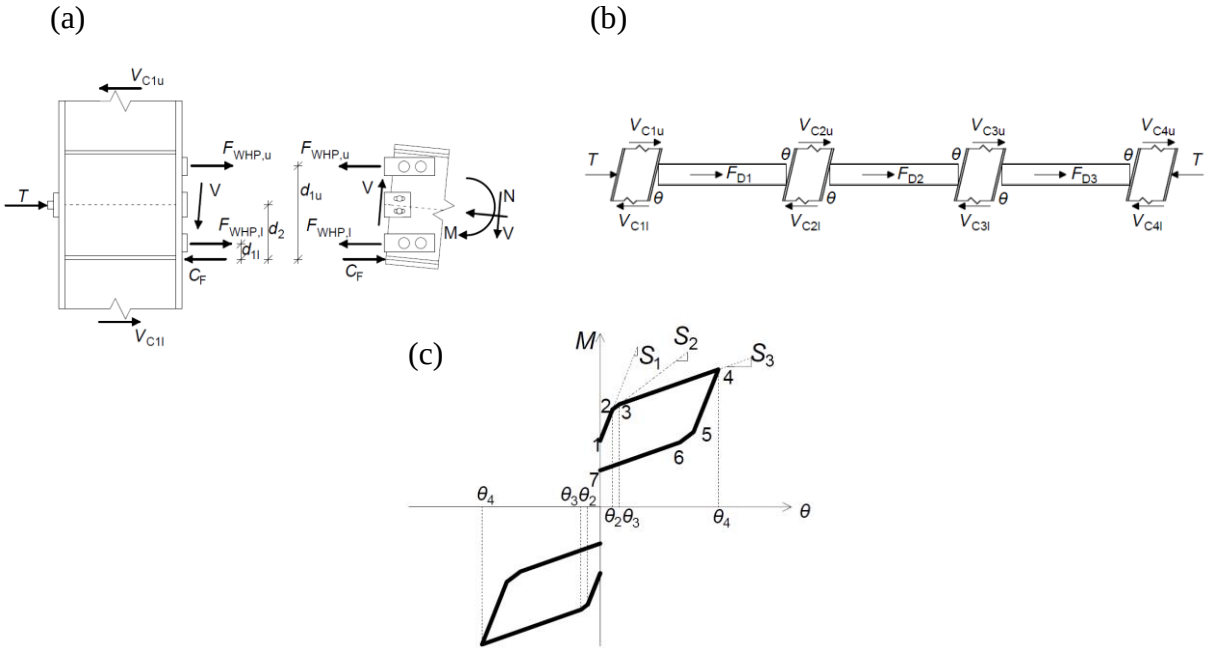

Figure 3: (a) Free body diagram of an external PT connection; and (b) SC-MRF expansion and horizontal forces equilibrium; (c) theoretical cyclic behaviour of the PT connections with WHPs.

3 ECONOMIC SEISMIC LOSS ESTIMATION

3.1 Economic seismic loss estimation framework

The seismic loss of a building is split into three distinct types according to ATC-58 [30]: (a) structural loss due to damage in load-carrying structural members; (b) non-structural loss due to damage in non-load carrying components such as partitions, piping systems, etc.; and (c) building contents loss. Such types of seismic loss are assessed using component fragility functions (e.g. cumulative lognormal distribution functions) parameterized on engineering demand parameters (EDPs) such as the peak storey drift ($\theta_{s,max}$) or the PFA. For a specific value of the chosen seismic intensity measure (IM), each component has a certain probability of being in any damage state (DS), which is then associated with a probabilistic cost function. Such function defines the cumulative distribution of the repair cost of the component for the given DS. Summing up all component costs over the entire building yields the total economic seismic loss. Following the guidelines of ATC-58 [30], the spectral acceleration at the fundamental period of vibration, $S_a(T_1)$, is chosen as IM.

3.2 Probability of collapse and probability of demolition

The probability of collapse can be explicitly incorporated in the economic seismic loss estimation framework following the methodology in [28], i.e. collapse is assumed to cause instant loss of the entire building and its contents. The probability of demolition is also incorporated following [31], i.e. by recognizing that the building will be demolished when a critical value of the residual storey drift ($\theta_{s,res}$) is exceeded. The probability of having to demolish the structure conditioned on $\theta_{s,res}$, $P(D|\theta_{s,res})$, is assumed to follow a lognormal distribution with a logarithmic standard deviation of 0.3 according to [31] and a median value that was assumed equal to 0.50% [33], 1.00% and 1.88% [32] to allow a parametric study to be conducted.

3.3 Vulnerability functions

Vulnerability functions are developed using the simulation procedure described in the PEER loss analysis framework [26, 35]. In the PEER framework, the mean annual frequency (MAF) of a decision variable (DV), such as the repair cost or the loss ratio (i.e. repair cost over the building replacement cost), is estimated as

$$\lambda_{DV}(DV \geq dv) = \int_{IM}\int_{DS}\int_{EDP} G(dv|DS)\left|dG(DS|EDP)\right|\left|dG(EDP|IM)\right|\left|\frac{d\lambda(IM)}{dIM}\right| dIM \quad (1)$$

where $\lambda_{DV}(DV \geq dv)$ is the MAF of exceeding dv (e.g. value of repair cost or loss ratio) for the given site and building; $G(dv|DS)$ is the probability of exceedance of dv given a DS (i.e. damage state associated with a specific repair action); $G(DS|EDP)$ is the probability of exceedance of DS given an EDP; $G(EDP|IM)$ is the probability of exceedance of EDP given an IM; and $\lambda(IM)$ is the MAF of exceedance of the IM.

In this work, only a part of Equation (1) is used to assess the performance of a building in an objective manner that does not depend on the site, i.e. using only the integrals of $G(dv|DS)$ over EDP and DS without the final convolution with $\lambda(IM)$. The result is known as the vulnerability function:

$$G(DV|IM) = \int_{DS}\int_{EDP} G(dv|DS)\left|dG(DS|EDP)\right|\left|dG(EDP|IM)\right| \quad (2)$$

Equation (2) computes DV as a function of IM and it is characteristic of the building and independent of the site (provided that a sufficient IM is used). With loss being an inherently probabilistic quantity, it is more accurate to discuss vulnerability functions for certain statistics of the loss in the structure. 16%, 50% and 84% are typically chosen fractile values of vulnerability given the IM level. Monte Carlo Simulation (MCS) is used to evaluate the integrals shown in Equation (2). The MCS approach involves several steps and simulates all the random variables in Equation (2) (i.e. DV, EDP, DS, IM) to finally compute DV for a wide range of IMs. The steps involved in the MCS approach are presented in detail in [32].

4 PROTOTYPE BUILDING AND DESIGN OF SEISMIC-RESISTANT FRAMES

Figure 4(a) shows the plan view of a 5-storey, 5-bay by 3-bay prototype building having two identical perimeter seismic-resistant frames in the 'x' plan direction. These frames are designed as conventional MRFs, MRFs with viscous damper, SC-MRFs and SC-MRFs with viscous dampers, based on existing design procedures [23, 24]. All the buildings are designed to have the same cross sections. In such a way buildings with different type of lateral-load resisting system will have the same fundamental period, but different structural performance under strong ground motions. Viscous dampers are installed in the interior gravity frames (with pinned beam-column and pinned column base connections) that are coupled with the perimeter seismic-resistant frames through the floor diaphragm as shown in figure 4(b). For all design cases $\theta_{s,max}$ is less than 0.75% under the frequently occurred earthquake (FOE) according to EC8 [24]. The DBE is expressed by the Type 1 elastic response spectrum of EC8 with peak ground acceleration equal to 0.35g and ground type B. The FOE has intensity of 40% (reduction factor v=0.4 in EC8) the intensity of the DBE. The maximum considered earthquake (MCE) has intensity of 150% the intensity of the DBE. The model used for the design is based on the centerline dimensions of the seismic-resistant frame without accounting for the finite panel zone dimensions. A 'lean-on' column is included in the model to account for the P-Δ effects of the vertical loads acting on the gravity columns in the tributary plan area (half of the total plan area) assigned to the seismic-resistant frame. A rigid diaphragm

constraint is imposed at the nodes of each floor level for the design. The steel yield strength is equal to 355 MPa for the columns, 275 MPa for beams, 930 MPa for PT bars, 235 MPa for the WHPs and 275 MPa for the beam reinforcing plates. Nonlinear viscous dampers are designed with a horizontal configuration (as shown in figure 4(b)) and a velocity exponent equal to 0.5 to achieve a total damping ratio equal to 20% at the first fundamental period, which is equal to T_1=1.27 s. The estimated $\theta_{s,max}$ under the DBE is equal to 1.20% and 1.80% for the frames with and without dampers, respectively. Design data of the frames are given in table 1.

To evaluate the performance of the prototype building of figure 4 in terms of repair and replacement cost, it is assumed that the building includes the structural components, non-structural components and contents listed in table 2. Table 2 lists the component, the associated ATC-58 [30] identification (ID), the component units that the building includes per storey, and the associated EDP used to assess the component DS.

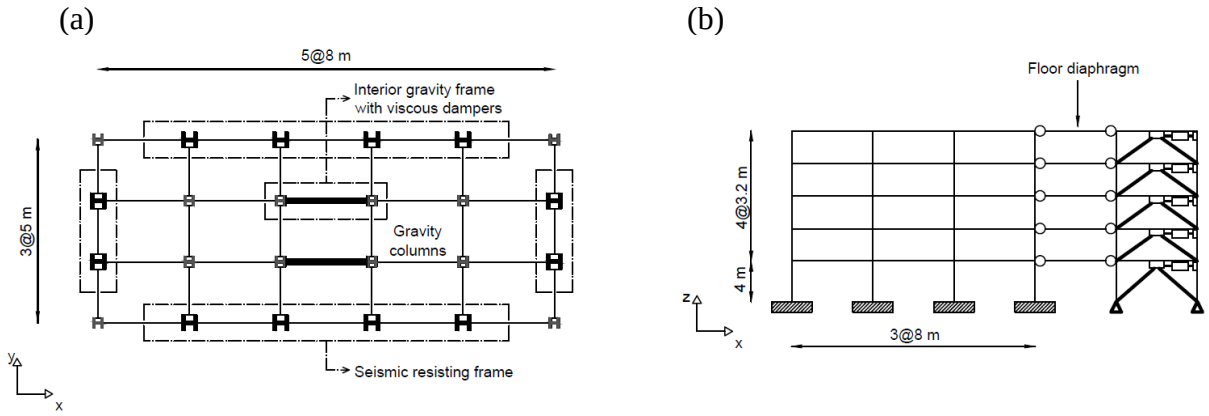

Figure 4: (a) Plan view of the prototype building; (b) Elevation view of the prototype building.

Table 1: Design data of the steel MRF, SC-MRF and viscous dampers

	Cross sectios		PT force	PT bar diameter	WHPs with L_{whp} = 70mm		Reinf. plate length	Reinf. plate thickness	Viscous dampers
Storey	Beam	Column	T_0 (kN)	d_{PT} (mm)	D_e (mm)	D_i (mm)	L_{rp} (mm)	t_{rp} (mm)	c (kN·(s./m)$^{0.5}$)
1	IPE550	HEB650	1087	50	43	33	1392	35	2139
2	IPE600	HEB650	1256	60	46	36	1660	46	1641
3	IPE550	HEB650	1087	48	43	33	1416	35	1416
4	IPE500	HEB600	941	38	41	30	1092	26	1102
5	IPE500	HEB600	941	36	39	28	743	22	810

The fragility and cost functions of the PT connections are not provided by ATC-58 [30]. On the basis of limited information, market research and engineering judgement are used to determine these functions. It is assumed that DSs in the PT connections are associated with the replacement of WHPs under the DBE and the plastic hinge rotation, θ_p, at the end of the reinforcing beam flange plate. θ_p is associated to $\theta_{s,max}$ on the basis of pushover analysis. PT bar yielding is not considered as a DS, because it is not critical failure mode in the current design cases (see Section 6.1). For the definition of fragility functions, equations presented in Chapter 3 of ATC-58 [30] are used. The cost functions related to the θ_p at the end of the reinforcing beam flange plate were determined based on the mean and dispersion values of the corresponding conventional moment resisting connections. The labour and material cost of the WHPs has been used for the definition of the DS associated with WHP replacement. The contents cost functions have been developed based on USA market prices.

5 MODELS FOR NONLINEAR ANALYSES

Models for the SC-MRFs are developed in OpenSees [36] as shown in figure 5. The columns and the reinforced lengths of the beams are modelled as nonlinear force-based beam-column fiber elements. Fibers have bilinear elastoplastic stress-strain behaviour (Steel01 in OpenSees) with post-yield stiffness ratio of 0.003. The assumption of stable hysteresis for the columns is fully justified as heavy columns with webs and flanges of low slenderness do not show cyclic deterioration even under large drifts [37].

Table 2: Prototype building components per storey

MRF components	**ATC-58 (ID)**	**SC-MRF components**	**nits**	**DP**
Steel column base plate	B103 1.011b	-//-		$_{s,max}$
Post-Northridge welded steel moment connection, beam one side	B103 5.021 / None	PT connection, beam one side		$_{s,max}$
Post-Northridge welded steel moment connection, beams both sides	B103 5.031 / None	PT connection, beams both sides		$_{s,max}$
Bolted shear tab gravity connections	B103 1.001	-//-	8	$_{s,max}$
curtain walls	B202 2.001	-//-	4	$_{s,max}$
suspended ceiling	C303 2.003a	-//-	6	FA
cold water piping	D202 1.011a	-//-		FA
hot water piping	D202 2.012b	-//-		FA
HVAC	D304 1.001a	-//-		FA
Modular office work stations	E202 2.001	-//-	0	FA
unsecured fragile objects on shelves	E202 2.010	-//-	0	FA
electronic equipment on wall	E202 2.021	-//-		FA
Desktop electronics	E202 2.022	-//-	0	FA
Book case	E202 2.102a	-//-	0	FA

Beam local buckling is expected just after the end of the reinforcing plates, and therefore, the unreinforced lengths of the beams are modelled using Force-based beams with hinges elements incorporating the modified Gauss–Radau plastic hinge integration method developed by Scott and Fenves [38]. The implementation divides the element into two hinges at the ends, with one integration point per hinge and a linear-elastic region in the middle with two integration points. Strength and stiffness deterioration model [39] is assigned on the beams fibers, according to [40]. This approach results in smooth backbone curves for flexural members, similar to that observed in experiments.

Panel zones are modelled using the Krawinkler model [41] which consists of four rigid links connected at the corners by rotational springs. The springs at the lower left and upper right corners have no stiffness, and thereby act as true hinges. The spring at the upper left is used to represent panel zone shear resistance, and the spring at the lower right is used to represent column flange bending resistance.

To account for P-Δ effects, the gravity columns associated with the SC-MRFs are modelled as lean-on columns. Diaphragm action is modelled with truss elements connecting the lean on columns nodes to nodes defined along the length of the beams at the points where secondary beams are placed. These trusses have stiffness of 100 times the axial beam stiffness.

Nonlinear viscous dampers are modelled with zero length elements (Viscous material of OpenSees), while their supporting braces are modelled with elastic braces as they are strong enough to avoid buckling. In the analytical model, the damper limit states caused by their stroke limit are not considered, i.e. it is assumed that dampers will be manufactured with enough stroke to avoid reaching their limit states even under very large storey drifts.

Models of PT connections with WHPs have been proposed in [10, 24]. In this work, a simplified modelling for PT connections has been adopted where the *M-θ* behaviour of the PT connection is simulated by inserting 2 rotational springs in parallel at the beams ends (see figure 5). These rotational springs simulate the contribution of the WHPs and the PT bars on the overall rotational behaviour of the PT connection. In this simplified modelling, the beams compressive axial forces due to PT bars tensile forces are not simulated.

The model with the simplified PT connections has been evaluated against the detailed model of [9, 23] with cyclic and monotonic pushover analyses. The results showed that the simplified model is capable to accurately simulate the frame response.

The connections of the conventional MRFs are assumed to be rigid and have full strength, while beams are modeled as elastic elements with zero length rotational springs at their ends that exhibit strength and stiffness deterioration [39]. Columns and panel zones are modeled as described above for the SC-MRFs.

The OpenSees models for the SC-MRFs and the conventional MRFs include the effect of the panel zone stiffness, and so, result in T_1 value shorter than 1.27 s that is based on the centerline models used for design. T_1 from the OpenSees models is 0.94 s for both SC-MRFs with and without viscous dampers and 1.18 s for both MRFs with and without viscous dampers.

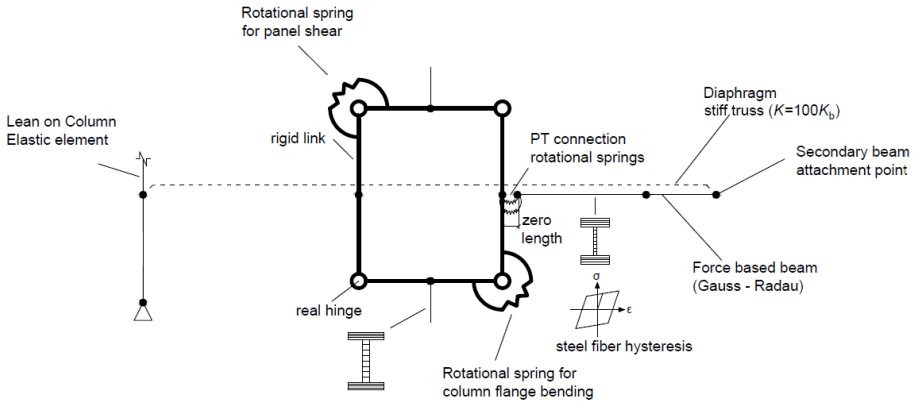

Figure 5: Simplified model for an exterior PT connection and the associated beams and columns.

6 NONLINEAR STATIC AND DYNAMIC ANALYSES

6.1 Nonlinear static analyses

Figure 6 shows the base shear coefficient (*V/W*; *V*: base shear and *W*: seismic weight) - roof drift (θ_r) behaviour of the SC-MRFs and the conventional MRFs from pushover analysis.

A displacement-controlled pushover analysis is executed up to θ_r of 10%. Pushover curves are shown along with structural limit states and θ_r estimations under the FOE, DBE and MCE.

Figure 6(a) shows the pushover curve of the SC-MRF. WHPs yield at θ_r equal to 0.2% lower than the FOE θ_r (0.6%) followed by column plastic hinge at θ_r equal to 1.0% before DBE θ_r (1.6%). Plastic hinge at the end of the beam flange reinforcing plate occurs at θ_r equal to 2.5% after MCE θ_r (2.4%). After this point the strength of SC-MRF continues to increase up to θ_r of 4.7% where beam local buckling occurs and strength deterioration initiates. PT bars do not yield even under very large drifts as the beam plastic hinge rotations drastically reduce gap opening and PT bar elongation. The peak *V/W* is 0.34. Viscous dampers do not affect the behaviour of the SC-MRFs under static loading, and so, SC-MRF with viscous dampers has the same pushover curve (figure 6(b)) with the SC-MRF apart from lower θ_r under the FOE, DBE and MCE. Column plastic hinge occurs at the DBE θ_r (1.0%), while beam plastic hinge occurs at θ_r higher than the MCE θ_r (1.6%).

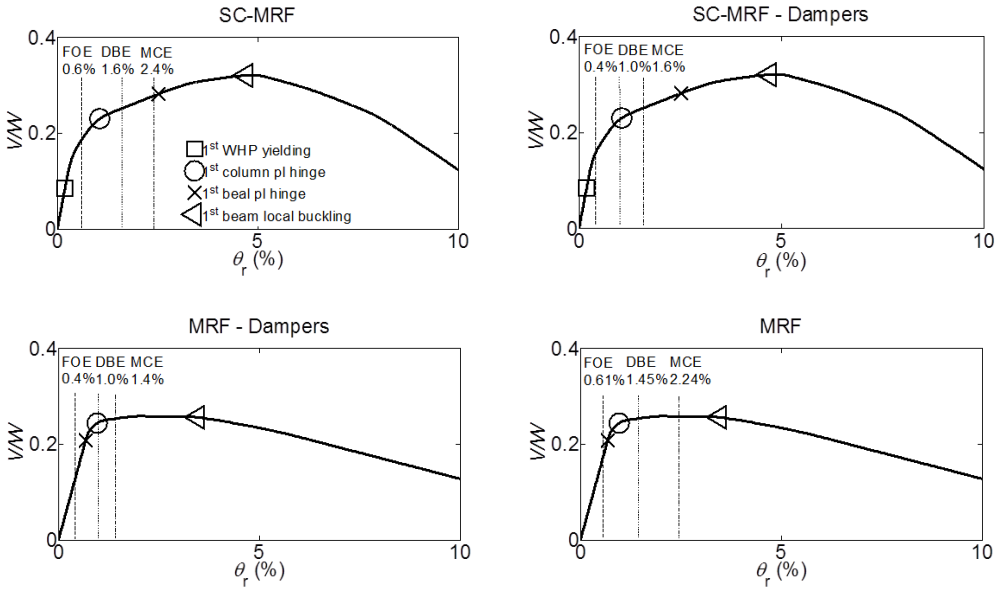

Figure 6: *V/W*-θ_r behaviour from nonlinear monotonic (pushover) static analysis.

Figure 6(c) shows the pushover curve of the conventional MRF. Beam plastic hinge occurs at 0.7% θ_r followed by column plastic hinge formation at 1.0% θ_r and beam local buckling at 3.4% θ_r. The behaviour of the conventional MRF is worse than the behaviour of the SC-MRF with the same cross-sections as all structural limit states are reached at lower θ_r. The peak *V/W* is 0.26. Viscous dampers do not affect the behaviour of the MRFs under static loading, and so, MRF with viscous dampers has the same pushover curve (Figure 6(d)) with the MRF apart from lower θ_r under the FOE, DBE and MCE. Column plastic hinge occurs at the DBE θ_r (1.0%), while beam plastic hinge occurs at θ_r in between the FOE θ_r (0.4%) and DBE θ_r (1.0%).

Figure 7 shows the *V/W*-θ_r behaviour of the SC-MRFs and the conventional MRF from nonlinear cyclic (push-pull) static analysis up to the DBE θ_r. SC-MRFs with and without viscous dampers have good energy dissipation capacity and self-centering capability. SC-MRF has a small residual θ_r due to modest column base yielding. The conventional MRFs with and without viscous dampers show higher energy dissipation capacity but have significant residual θ_r compared to all SC-MRFs.

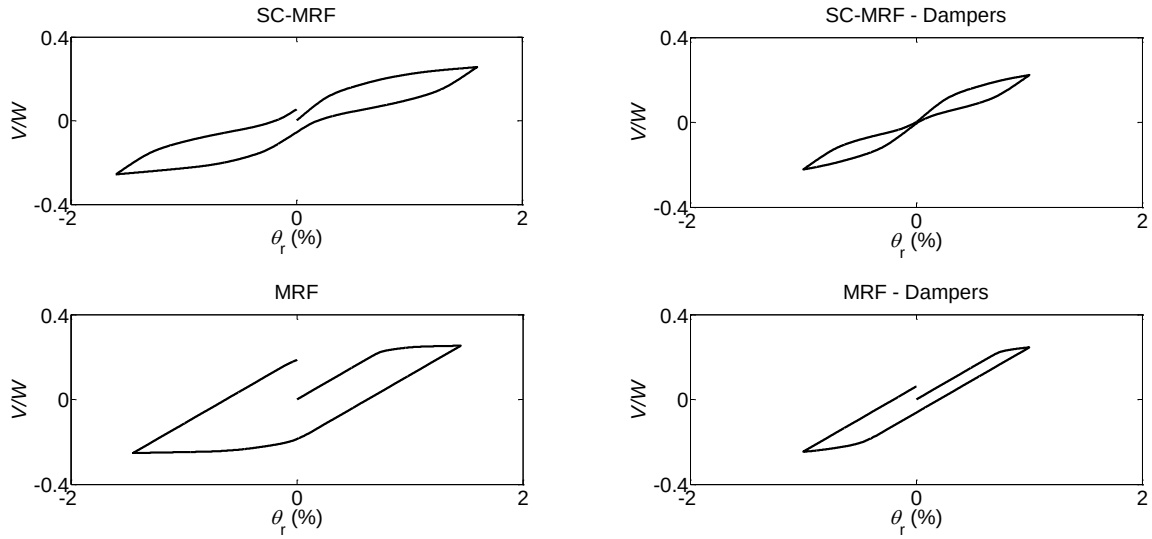

Figure 7: V/W-θ_r behaviour from nonlinear cyclic (push-pull) static analysis up to DBE roof drift.

6.2 Nonlinear dynamic analyses – collapse simulation

To investigate sidesway collapse, incremental dynamic analysis (IDA) [42] is performed for all the deign cases (SC-MRF, SC-MRF with viscous dampers, MRF, and MRF with viscous dampers). IDA involves increased amplitude scaling of individual ground motion records to estimate the relationship between IM and EDP. For the IDA simulations, sidesway collapse is defined as the point of dynamic instability when $\theta_{s,max}$ increases without bound. IDAs were performed under a set of 22 recorded far-field ground motions pairs (i.e. 44 time histories) developed by the ATC-63 [43] project. The Newmark method with constant acceleration is used to integrate the equation of motions. A Rayleigh damping matrix is used to model the inherent 3% critical damping at the first two modes of vibration. Each dynamic analysis is extended well beyond the actual earthquake time to allow for damped free vibration decay and accurate $\theta_{s,res}$ calculation. Figure 8 shows the IDA curves of all the design cases.

Having $S_a(T_1)$ collapse of the SC-MRF from the IDA curves (figure 8(a)), a fragility curve is constructed by fitting a lognormal cumulative distribution function to define the probability of collapse as a function of $S_a(T_1)$, as shown in figure 9(a). Figure 9(b) shows the collapse fragility curves of all the design cases, where the $S_a(T_1)$ is normalized by $S_{a,MCE}$, i.e. the MCE spectral acceleration of the ground motion at T_1. $S_{a,MCE}$ equals to 0.83g for the SC-MRF, 0.53g for SC-MRF with viscous dampers, 0.67g for MRF and 0.42g for MRF with viscous dampers. All the examined design cases, shown in figure 9(b), have superior collapse resistance, with zero probability of collapse under the MCE. SC-MRF has significantly better performance with fragility curves clearly shifted to the right of the MRF. The median collapse capacity $S_a(T_1)$ equals to $4.5 \cdot S_{a,MCE}$ for the SC-MRF and $3.6 \cdot S_{a,MCE}$ for MRF. The use of viscous dampers results in higher collapse resistance for both the MRF and the SC-MRF, with the corresponding collapse fragility curves shifted to the right. The median collapse capacity $S_a(T_1)$ equals to $8.6 \cdot S_{a,MCE}$ and $8.0 \cdot S_{a,MCE}$ for the SC-MRF with viscous dampers and MRF with viscous dampers, respectively.

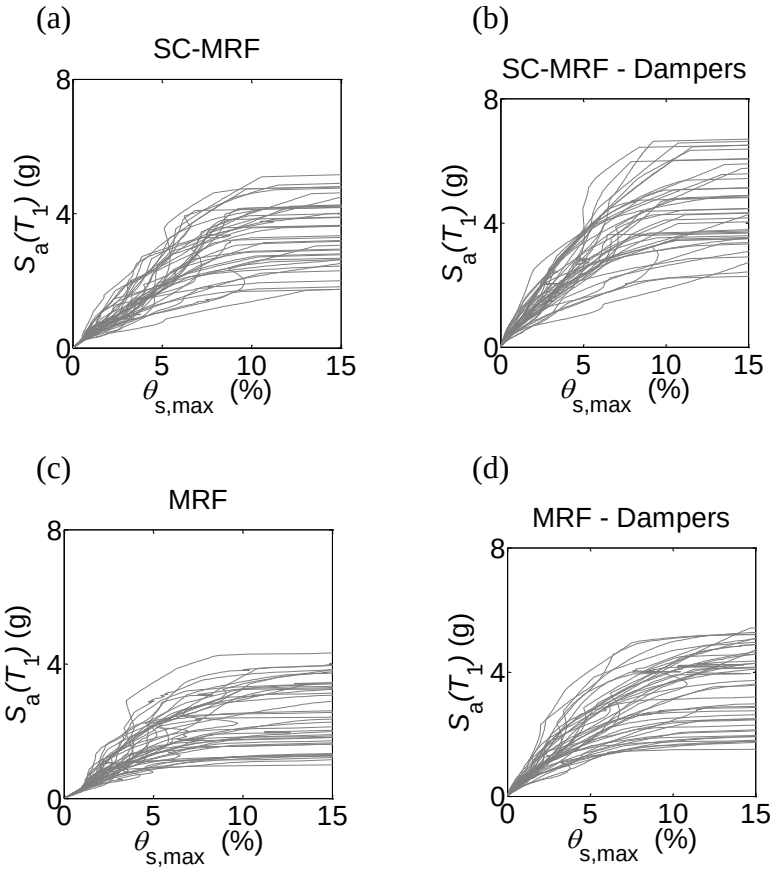

Figure 8: (a) IDAs of SC-MRF; (b) IDAs of SC-MRF with viscous dampers; (c) IDAs of MRF; and (d) IDAs of MRF with viscous dampers.

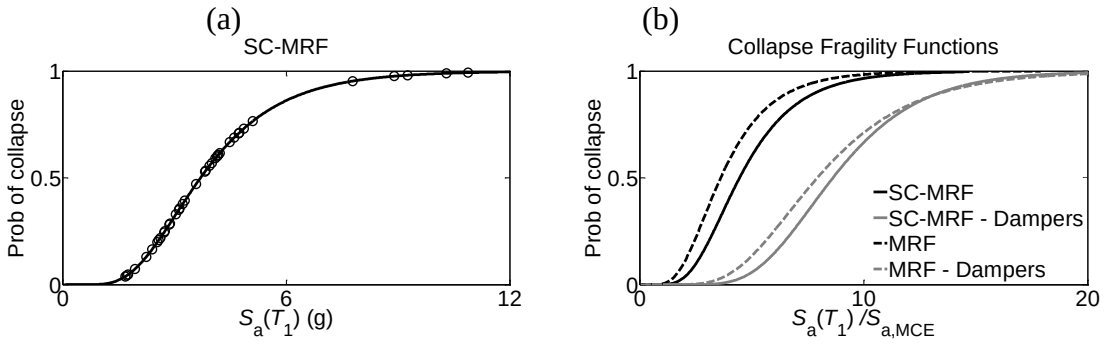

Figure 9: (a) Collapse fragility function of SC-MRF; (b) Collapse fragility function of all design cases, normalized to $S_{a,MCE}$.

7 ESTIMATION OF ECONOMIC SEISMIC LOSSES

7.1 Vulnerability functions

The vulnerability functions of this Section are derived by assuming that the median and lognormal standard deviation of $P(D|\theta_{s,res})$ are equal to 1.88% [32] and 0.30 [31], respectively. Figure 10 shows the vulnerability functions of all the design cases, at 16%, 50% and 84% probability of exceedance of a DV for a wide range of IMs. The selected DVs are the repair cost and the loss ratio.

The SC-MRFs with and without viscous dampers have better performance compared to the corresponding MRFs, with their vulnerability function shifted to the top of figure 10. Also, both MRF and SC-MRF have better performance when viscous dampers are inserted into the building. The SC-MRF with viscous dampers has higher performance with vulnerability functions clearly shifted to the top of those of the other frames. This demonstrates the effectiveness of supplemental damping to improve the structural and non-structural seismic performance of steel SC-MRFs by minimize $\theta_{s,res}$ under high seismic intensities. The 50% probability of repair cost to be exceeded for each design case is presented in table 3, under several seismic intensities.

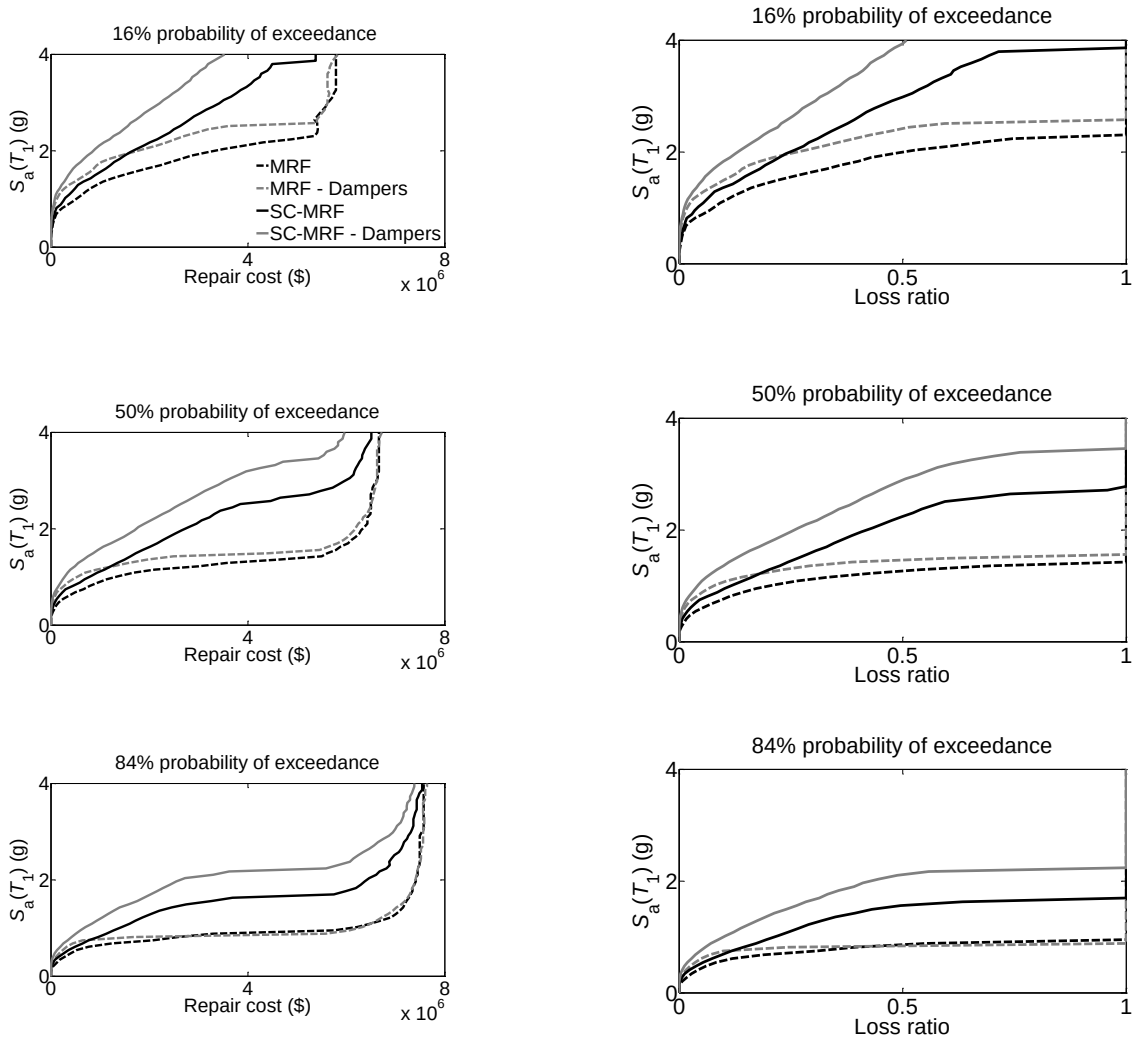

Figure 10: 16%, 50% and 84% probability of a DV to be exceeded, expressed in terms of repair cost and loss ratio, for a wide range of IMs.

The results in table 3 show that viscous dampers reduce by more than 90% the repair cost for both MRF and SC-MRF under the MCE and DBE, while they minimize it under the FOE. SC-MRFs with and without viscous dampers have similar performance with the corresponding MRFs, under the FOE, DBE and MCE. For $S_a(T_1)$=1.0g the repair cost of both MRF and SC-MRF is reduced by more than 50% when viscous dampers are inserted into the building; SC-MRFs with and without viscous dampers reduce the repair cost by 50% and 40% compared to the corresponding MRFs, respectively. For $S_a(T_1)$=2.0g and $S_a(T_1)$=3.0g, viscous dampers are more effective into the SC-MRF. For $S_a(T_1)$=2.0g the SC-MRFs with and without

viscous dampers reduce the repair cost by 72% and 56% compared to the corresponding MRFs, respectively. For $S_a(T_1)$=3.0g the SC-MRF with viscous dampers has significantly better performance than the other design cases (45% reduction in repair cost). The aforementioned results demonstrate the crucial role of $\theta_{s,res}$ by considering the losses resulting from the $P(D|\theta_{s,res})$ (as discussed in Section 3.2) and the ability of the SC-MRFs to reduce the repair cost by minimize $\theta_{s,res}$, under high seismic intensities.

Table 3: 50% probability of repair cost to be exceeded in \$ (10^6). Buildings with contents and median of $P(D|\theta_{s.res.max})$ equal to 1.88%

Design cases	$S_{a,FOE}$	$S_{a,DBE}$	$S_{a,MCE}$	$S_a(T_1)$=1.0g	$S_a(T_1)$=2.0g	$S_a(T_1)$=3.0g
MRF	0.01	0.15	0.50	1.39	6.37	6.64
MRF - Dampers	0.00	0.01	0.02	0.57	6.20	6.63
SC-MRF	0.01	0.13	0.45	0.82	2.80	6.07
SC-MRF - Dampers	0.00	0.01	0.04	0.29	1.78	3.67

7.2 Sensitivity of loss to changes in the probability of demolition

In Sections 7.1 it was assumed that the $P(D|\theta_{s,res})$ follows a lognormal distribution, with median equal to 1.88% [32] and logarithmic standard deviation 0.3 [31]. However, there are limited data available and limited information about the statistical parameters of this distribution. In this Section a sensitivity analysis was conducted to examine how different estimates of the median of $P(D|\theta_{s,res})$ affect the estimation of the economic losses.

To examine the sensitivity of the economic losses to the median of $P(D|\theta_{s,res})$, additional loss analyses were conducted using medians of $P(D|\theta_{s,res})$ equal to 0.5% [33] and 1.0% while holding the dispersion constant at 0.30, since loss estimations are much more sensitive to changes in the median than the dispersion of the probability of demolition [31]. Figures 11 and 12 show the vulnerability functions of all the design cases for median of $P(D|\theta_{s,res})$ equal to 0.5% and 1.0%, respectively. In figures 11 and 12, only the 50% probabilities of a DV to be exceeded for a wide range of IMs are presented. The selected DVs are the repair cost and the loss ratio.

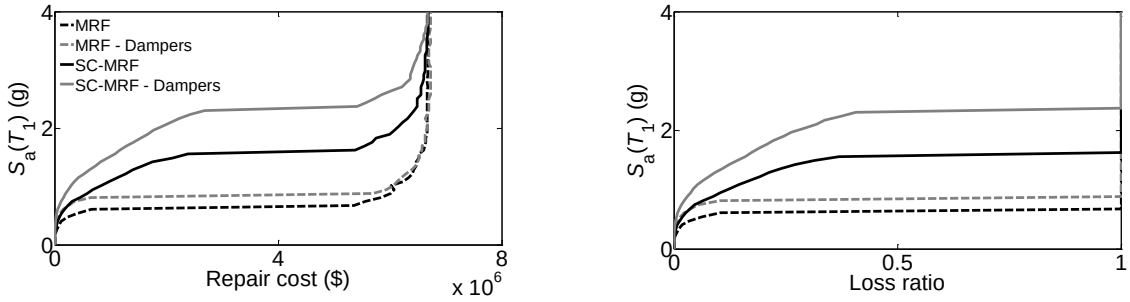

Figure 11: 50% probability of repair cost and loss ratio to be exceeded for median of $P(D|\theta_{s,res})$ equal to 0.5%.

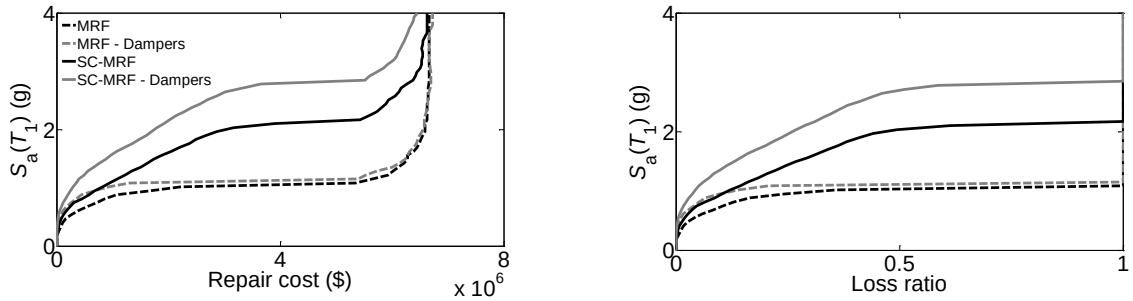

Figure 12: 50% probability of repair cost and loss ratio to be exceeded for median of $P(D|\theta_{s,res})$ equal to 1.0%.

Table 4: 50% probability of repair cost to be exceeded in \$ (10^6). Buildings with median of $P(D|\theta_{s.res.max})$ equal to 0.5%

Design cases	$S_{a,FOE}$	$S_{a,DBE}$	$S_{a,MCE}$	$S_a(T_1)$=1.0g	$S_a(T_1)$=2.0g	$S_a(T_1)$=3.0g
MRF	0.01	0.14	5.36	6.02	6.67	6.68
MRF - Dampers	0.00	0.01	0.03	6.06	6.67	6.73
SC-MRF	0.01	0.13	0.45	0.83	6.15	6.63
SC-MRF - Dampers	0.00	0.01	0.04	0.29	1.92	6.41

The results in table 4 show that viscous dampers minimize the repair cost for both MRF and SC-MRF under the FOE, DBE and MCE. The SC-MRFs with and without viscous dampers have similar performance with the corresponding MRFs, under the FOE and DBE. Under the MCE, the SC-MRF has a significantly reduced repair cost (90%) than the MRF, while the SC-MRF with viscous dampers has similar performance with the MRF with viscous dampers. For $S_a(T_1)$=1.0g and $S_a(T_1)$=2.0g viscous dampers are more effective only into the SC-MRF, where they result in 69% reduction of repair cost, while the repair cost of the MRF does not significantly changes when viscous dampers are inserted. In addition, for $S_a(T_1)$=1.0g the SC-MRFs with and without viscous dampers reduce the repair cost by 95% against the corresponding MRFs with and without viscous dampers. For $S_a(T_1)$=2.0g the SC-MRF with and without viscous dampers reduce the repair cost by 72% and 10% against the MRFs with and without viscous dampers respectively. For $S_a(T_1)$=3.0g viscous dampers are not effective for both MRF and SC-MRF, while the SC-MRF with and without viscous dampers has similar performance with the MRFs with and without viscous dampers, respectively.

Table 5: 50% probability of repair cost to be exceeded in \$ (10^6). Buildings with median of $P(D|\theta_{s.res.max})$ equal to 1.0%

Design cases	$\boldsymbol{S_{a,FOE}}$	$\boldsymbol{S_{a,DBE}}$	$\boldsymbol{S_{a,MCE}}$	$\boldsymbol{S_a(T_1)}$**=1.0g**	$\boldsymbol{S_a(T_1)}$**=2.0g**	$\boldsymbol{S_a(T_1)}$**=3.0g**
MRF	0.01	0.14	5.36	6.02	6.67	6.68
MRF - Dampers	0.00	0.01	0.03	6.06	6.67	6.73
SC-MRF	0.01	0.13	0.45	0.83	6.15	6.63
SC-MRF - Dampers	0.00	0.01	0.04	0.29	1.92	6.41

The results in table 5 show that viscous dampers minimize the repair cost under the FOE, DBE and MCE. The SC-MRFs with and without viscous dampers have similar performance with the corresponding MRFs, under the FOE. Under the DBE and MCE, the SC-MRF has reduced repair cost compared to MRF by 20% and 17%, respectively, while the SC-MRF with viscous dampers has similar performance with the MRF with viscous dampers. For $S_a(T_1)$=1.0g viscous dampers reduce the repair cost by 58% and 65% for the MRF and SC-MRF, respectively; SC-MRFs with and without viscous dampers reduce the repair cost by 69% and 63% compared to MRFs with and without viscous dampers, respectively. For $S_a(T_1)$=2.0g and $S_a(T_1)$=3.0g viscous dampers are more effective only into the SC-MRF,

where they result in 28% and 10% reduction of repair cost respectively, while the repair cost of the MRF does not significantly changes when viscous dampers are inserted; SC-MRFs with and without viscous dampers reduce the repair cost by 73% and 52% compared to the corresponding MRFs, respectively. For $S_a(T_1)$=3.0g the SC-MRF has similar performance with the MRFs, while the repair cost of the SC-MRF with viscous dampers is reduced by 16% compared to MRF with viscous dampers.

Comparison between the results of table 4 and 5 shows that by using median of $P(D|\theta_{s,res})$ equal to 0.5%, the SC-MRF has 90% reduced repair cost compared to the MRF repair cost under the MCE, while by using median of $P(D|\theta_{s,res})$ equal to 1.0%, the SC-MRF has 20% and 17% reduced repair cost under the DBE and MCE, respectively. In addition, the results of Table 3 show that by using median of $P(D|\theta_{s,res})$ equal to 1.88% both MRF and SC-MRF under the MCE and DBE have similar repair cost. The aforementioned results demonstrate the crucial role of $\theta_{s,res}$ by considering the losses resulting from the $P(D|\theta_{s,res})$, since it can affect the selected type of lateral resisting system. Nevertheless, more work is needed to evaluate the $\theta_{s,res}$ beyond which the structure can be demolished.

8 CONCLUSION

In this paper the potential of SC-MRFs with viscous dampers to reduce the economic losses in steel buildings due to strong earthquakes is evaluated. The evaluation is based on the comparison of different designs of a prototype steel building using as lateral-load resisting system: 1) conventional steel MRFs; 2) MRFs and viscous dampers; 3) SC-MRFs; and 4) SC-MRFs with viscous dampers. The building's repair cost is evaluated by developing vulnerability functions according to the state of the art ATC-58 methodology, and compared for all the design cases. The probability of demolition after a strong earthquake was also taken into account by assuming different permissible residual storey drifts levels. Based on the results presented in the paper, the following conclusions are drawn:

1. All the examined design cases have zero probability of collapse under the MCE. The SC-MRF has higher collapse resistance compared to the corresponding MRF. The use of viscous dampers results in higher collapse resistance for both the MRF and the SC-MRF, while the SC-MRF with viscous dampers has superior collapse resistance.
2. The use of viscous dampers reduces the repair cost by more than 90% for both the MRF and SC-MRF under the MCE and DBE, while the repair cost is minimized under the FOE.
3. SC-MRFs with and without viscous dampers have similar performance to that of the corresponding MRFs, up to the MCE. For higher seismic intensities (e.g. $S_a(T_1)$=2.0g), SC-MRFs with and without dampers have significantly improved performance compared to the corresponding MRFs and lower repair cost, while the effect of dampers is considerable in the case of the SC-MRF.
4. Supplemental viscous damping is very effective in improving the residual drift performance and reduces the economic losses for both the SC-MRF and MRF.
5. The results highlight the importance of considering residual drifts as a demand parameter controlling whether a building is repairable or needs to be demolished in the aftermath of a strong earthquake.
6. The selection of low median of probability of having to demolish the structure conditioned the residual storey, $P(D|\theta_{s,res})$, can justify the increased cost and design complexity of SC-MRFs with or without dampers, as lateral resisting systems. However, the selection of high median of $P(D|\theta_{s,res})$ can result to similar economic losses in both MRFs and SC-MRFs for seismic intensities up to MCE. In such cases MRFs with or without dampers can be more a economical design solution as lateral resisting systems.

7. Additional research is needed to evaluate the effect of the residual drift limit value beyond which the structure is demolished. Reliable values for this limit are needed to enhance the accuracy of loss estimation procedures.

ACKNOWLEDGEMENTS

This research has been supported by a Marie Curie Intra European Fellowship within the 7th European Community Framework Programme and by the Engineering and Physical Sciences Research Council of the United Kingdom (Grant Ref: EP/K006118/1).

REFERENCES

[1] New Zealand 2013 Treasury Budget Speech. http://www.treasury.govt.nz/budget/2013/speech/06.htm.

[2] Canterbury Earthquake Recovery Authority. http://cera.govt.nz/news/2014/new-program-to-show-progress-of-public-projects-14 may-2014.

[3] Ricles J., Sause R., Garlock M. and Zhao C., "Posttensioned seismic-resistant connections for steel frames". *Journal of Structural Engineering*, 127(2), 113-121, 2001.

[4] Christopoulos C., Filiatrault A., Uang C.M. and Folz B., "Posttensioned energy dissipating connections for moment-resisting steel frames", *Journal of Structural Engineering*, 128(9), 1111-1120, 2002.

[5] Chou C.C. and Lai Y.J., "Post-tensioned self-centering moment connections with beam bottom flange energy dissipators", *Journal of Constructional Steel Research*, 65(10-11), 1931-1941, 2009.

[6] Chou C.-C., Tsai K.-C. and Yang W.-C., "Self-centering steel connections with steel bars and a discontinuous composite slab", *Earthquake Engineering and Structural Dynamics*, 38, 403-422, 2009.

[7] Vasdravellis G., Karavasilis T.L. and Uy B., "Large-scale experimental validation of steel post-tensioned connections with web hourglass pins", *Journal of Structural Engineering*, 139(6), 1033-1042, 2013.

[8] Vasdravellis G., Karavasilis T.L. and Uy B., "Finite element models and cyclic behaviour of self-centering post-tensioned connections with web hourglass pins", *Engineering Structures*, 52:1-16, 2013.

[9] Dimopoulos A., Karavasilis T.L., Vasdravellis G. and Uy B., "Seismic design, modelling and assessment of self-centering steel frames using post-tensioned connections with web hourglass shape pins", *Bulletin of Earthquake Engineering*, 11, 1797–1816, 2013.

[10] Rojas P., Ricles J.M. and Sause R., "Seismic performance of post-tensioned steel moment resisting frames with friction devices", *Journal of Structural Engineering*, 131(4), 529-540, 2004.

[11] Kim H.J. and Christopoulos C., "Friction damped posttensioned self-centering steel moment-resisting frames", *Journal of Structural Engineering*, 134(11), 1768-1779, 2008.

[12] Tsai K.C., Chou C.C., Lin C.L., Chen P.C. and Jhang S.J., "Seismic self-centering steel beam-to-column moment connections using bolted friction devices", *Earthquake Engineering and Structural Dynamics*, 37, 627-645, 2008.

[13] Wolski M., Ricles J.M. and Sause R., "Experimental study of a self-centering beam-column connection with bottom flange friction device", *Journal of Structural Engineering*, 135(5): 479-488, 2009.

[14] Garlock M., Sause R. and Ricles J.M., "Behavior and design of posttensioned steel frame systems", *Journal of Structural Engineering*, 133(3), 389-399, 2007.

[15] Kim H.J. and Christopoulos C., "Seismic design procedure and seismic response of post-tensioned self-centering steel frames", *Earthquake Engineering and Structural Dynamics*, 38(3), 355-376, 2008.

[16] Karavasilis T.L., Sause R. and Ricles J.M., "Seismic design and evaluation of steel MRFs with compressed elastomer dampers", *Earthquake Engineering and Structural Dynamics*, 41(3), 411-429, 2012.

[17] Karavasilis T.L., Ricles J.M., Sause R. and Chen C., "Experimental evaluation of the seismic performance of steel MRFs with compressed elastomer dampers using large-scale real-time hybrid simulation", *Engineering Structures*, 33(6), 1859-1869, 2011.

[18] Karavasilis T.L., Kerawala S. and Hale E., "Model for hysteretic behaviour of steel energy dissipation devices and evaluation of a minimal-damage seismic design approach for steel frames", *Journal of Constructional Steel Research*, 70, 358-367, 2012.

[19] Karavasilis T.L. and Seo C.-Y., "Seismic structural and non-structural performance evaluation of highly damped self-centering and conventional systems", *Engineering Structures*, 33, 2248-2258, 2011.

[20] Seo C.-Y., Karavasilis T.L., Ricles J.M. and Sause R., "Seismic performance and probabilistic collapse resistance assessment of steel moment resisting frames with fluid viscous dampers", *Earthquake Engineering and Structural Dynamics*, 43(14), 2135-2154, 2014.

[21] Kurama Y.C., "Seismic design of unbonded post-tensioned precast concrete walls with supplementary viscous damping", *ACI Structural Journal*, 97(3), 648–658, 2000.

[22] Kam W.Y., Pampanin S., Palermo A. and Car A.J., "Self-centering structural systems with combination of hysteretic and viscous energy dissipations", *Earthquake Engineering and Structural Dynamics*, 39(10), 1083-1108, 2010.

[23] Tzimas A.S., Dimopoulos A.I. and Karavasilis T.L., "EC8-based seismic design and assessment of self-centering post-tensioned steel frames with viscous dampers", *Journal of Constructional Steel Research*, 105, 60-73, 2015.

[24] Eurocode 8 (EC8), *Design of structures for earthquake resistance*, 2013.

[25] Porter K.A., Kiremidjian A.S. and LeGrue JS., "Assembly-based vulnerability of buildings and its use in performance evaluation", *Earthquake Spectra* 2001, 17(2), 291-312, 2001.

[26] Cornell C.A. and Krawinkler H., "Progress and challenges in seismic performance assessment. *PEER Center News*, 3(2), 1–4, 2000.

[27] Porter, K.A., Beck, J.L. and Shaikhutdinov, R.V., "Sensitivity of building loss estimates to major uncertain variables", *Earthquake Spectra*, 18 (4), 719-743, 2002.

[28] Aslani H. and Miranda E., *Probabilistic earthquake loss estimation and loss disaggregation in buildings, Report No. 157*, The John A. Blume Earthquake Engineering Research Center, Stanford University, Stanford, CA, 2005.

[29] Gunay S. and Mosalam K.M., "PEER Performance-Based Earthquake Engineering Methodology, Revisited", *Journal of Earthquake Engineering*, 17, 829-858, 2013.

[30] Applied Technology Council (ATC), *ATC-58: Guidelines for Seismic Performance Assessment of Buildings*, 100% Draft. Redwood City, CA, 2012.

[31] Ramirez C.M. and Miranda E., "Significance of residual drifts in building earthquake loss estimation", *Earthquake Engineering and Structural Dynamics*, 41, 1477-1493, 2012.

[32] Jayaram N., Shome N. and Rahnama M., "Development of earthquake vulnerability functions for tall buildings", *Earthquake Engineering and Structural Dynamics*, 41, 1495-1514, 2012.

[33] McCormick J., Aburano H., Ikenaga M, and Nakashima M., "Permissible residual deformation levels for building structures considering both safety and human elements", *Proc. 14th world conference in Earthquake Engineering*, Seismological Press of China, Paper ID 05-06-0071, Beijing, 2008.

[34] Vasdravellis G., Karavasilis T.L. and Uy B., "Design rules, experimental evaluation, and fracture models for high-strength and stainless steel hourglass shape energy dissipation devices", *Journal of Structural Engineering* 2014; in press.

[35] Deierlein G.G., "Overview of a comprehensive framework for earthquake performance assessment", *Technical report, International Workshop on Performance-Based Seismic Design Concepts and Implementation*, Bled, Slovenia, 2004.

[36] OpenSees, *Open system for earthquake engineering simulation*, Pacific Earthquake Engineering Research Center, University of California at Berkeley, Berkeley, CA, 2013.

[37] Newell J. and Uang C.-M., "Cyclic behavior of steel wide-flange columns subjected to large drift", *Journal of Structural Engineering*, 134, 1334-1342, 2008.

[38] Scott M.H. and Fenves GL., "Plastic hinge integration methods for force –based beam-column elements. *Journal of Structural Engineering*, 132(2), 244-252, 2006.

[39] Lignos D.G., Krawinkler H, *A database in support of modeling of component deterioration for collapse prediction of steel frame structures*, ASCE Structures Congress, SEI institute, Long Beach CA, 2007.

[40] Hamidia M., Filiatrault A. and Aref A., "Simplified seismic sidesway collapse analysis of frame buildings", *Earthquake engineering and structural dynamics*, 43, 429-448, 2014.

[41] Krawinkler H., "Shear in Beam-Column joints in Seismic Design of Frames", *Engineering Journal*, 15(2) AISC, Chicago, Illinois, 1978.

[42] Vamvatsikos D. and Cornell C.A., "Incremental dynamic analysis", *Earthquake Engineering and Structural Dynamics*, 31(3), 491-514, 2002.

[43] FEMA P695, *Quantification of building seismic performance factors*, *ATC-63 Project*, Applied Technology Council, CA. USA, 2008.